AIAA JOURNAL
Vol. 38, No. 10, October 2000

Parabolized Navier–Stokes Algorithm for Solving Supersonic Flows with Upstream Influences

James H. Miller* and John C. Tannehill†
Iowa State University, Ames, Iowa 50011
and
Scott L. Lawrence‡
NASA Ames Research Center, Moffett Field, California 94035

A new parabolized Navier–Stokes (PNS) algorithm has been developed to efficiently compute supersonic flows with embedded regions that produce upstream effects. Innovative techniques are used to automatically detect and measure the extent of the embedded regions. Within the embedded regions, the PNS equations are globally iterated to duplicate the results that would be obtained with the complete Navier–Stokes (NS) equations. Once an embedded region is computed, the algorithm returns to the standard space-marching PNS mode until the next embedded region is encountered. This procedure has been successfully incorporated into NASA's upwind PNS code and it has been validated by its application to several two-dimensional test cases. All of these test cases include embedded regions that produce significant upstream effects. The present numerical results are in excellent agreement with previous NS computations and experimental data. In addition, these calculations demonstrate the significant reduction in computer time and storage that can be achieved by the use of this approach.

Introduction

THE parabolized Navier–Stokes (PNS) equations can be used to predict three-dimensional, steady, supersonic/hypersonic, viscous flowfields in an efficient manner.[1,2] This efficiency is achieved because the equations can be solved using a space-marching technique as opposed to the time-marching technique that is normally employed for the complete Navier–Stokes (NS) equations. As a result, the computational effort required to solve the PNS equations for an entire supersonic flowfield is similar to the effort required to solve either the inviscid portion of the flowfield by the use of the steady Euler equations or the viscous portion of the flowfield by the use of the boundary-layer equations. Furthermore, because the PNS equations contain all of the terms in both the Euler equations and the boundary-layer equations, the interaction between the inviscid and viscous portions of the flowfield is automatically taken into account.

Despite their efficiency, one of the major drawbacks of current day PNS codes is that they cannot be used to compute flows with embedded separated regions that occur near canopies, wing–body junctures, blunt leading edges, etc. A common practice is to use an NS code in these regions and use a PNS code for the remainder of the flowfield (see, for example, Ref. 3). Because of the difficulties associated with interfacing two different codes, other investigators have resorted to using an NS code for the entire flowfield. This is in spite of a typical PNS code being one to two orders of magnitude faster than a NS code and requiring substantially less computer storage.

An alternative approach that has been used by several investigators[4–11] is to modify an NS code so that it can space march the solution in supersonic regions. The drawback to this approach is that the NS equations are usually iterated several times at each streamwise step as the solution is marched downstream. It has been shown[10,12] that NS codes that have been modified in this fashion are substantially slower than a PNS code in supersonic regions. Because the majority of the inviscid flowfield surrounding a high-speed vehicle is supersonic, it seems advantageous to utilize a PNS code as the primary flow solver. This is the approach that is taken in the present study.

For a PNS-type code to be able to solve the entire flowfield surrounding a supersonic/hypersonic vehicle, it must be able to automatically detect and measure the extent of embedded regions that produce significant upstream effects. In the present study, an innovative technique has been developed to automatically detect and measure the extent of these embedded regions by the examination of the known body geometry and by the use of empirically determined correlation functions. In these embedded elliptic regions, the single-sweep space-marching technique is ill posed and inaccurate. Instead, the PNS equations must be solved globally in an iterative fashion to duplicate the results that would be obtained with an NS code. Once the embedded region is computed, the code can return to a space-marching mode until the next embedded region is encountered.

In the present study, a new iterative PNS (IPNS) algorithm has been developed to globally solve the governing equations in regions that have been determined to produce significant upstream effects. This algorithm has been incorporated into NASA's upwind PNS (UPS) code[13,14] and has been validated by its application to several two-dimensional laminar flow test cases that contain embedded regions with significant upstream effects. These test cases include supersonic flows over ramps and expansion corners, shock waves impinging on a flat plate, and flow over a more complicated geometry with two embedded regions. The present numerical results are compared with previous NS computations and experimental data for accuracy and computational efficiency.

PNS Equations

The PNS equations are obtained from the compressible NS equations by neglecting the streamwise viscous terms and by dropping the unsteady terms. The PNS equations expressed in a general nonorthogonal coordinate system (ξ, η, ζ) are given by

$$\boldsymbol{E}_\xi + \boldsymbol{F}_\eta + \boldsymbol{G}_\zeta = 0 \tag{1}$$

where

$$\boldsymbol{E} = (\xi_x/J)\boldsymbol{E}_i + (\xi_y/J)\boldsymbol{F}_i + (\xi_z/J)\boldsymbol{G}_i$$

$$\boldsymbol{F} = (\eta_x/J)(\boldsymbol{E}_i - \boldsymbol{E}_v') + (\eta_y/J)(\boldsymbol{F}_i - \boldsymbol{F}_v') + (\eta_z/J)(\boldsymbol{G}_i - \boldsymbol{G}_v')$$

$$\boldsymbol{G} = (\zeta_x/J)(\boldsymbol{E}_i - \boldsymbol{E}_v') + (\zeta_y/J)(\boldsymbol{F}_i - \boldsymbol{F}_v') + (\zeta_z/J)(\boldsymbol{G}_i - \boldsymbol{G}_v') \tag{2}$$

Received 4 May 1998; revision received 17 September 1999; accepted for publication 13 March 2000.

*Postdoctoral Research Associate, Department of Aerospace Engineering and Engineering Mechanics; currently Visiting Scientist, U.S. Air Force Research Laboratory, Wright–Patterson AFB, OH 45433. Senior Member AIAA.

†Manager, Computational Fluid Dynamics Center, and Professor of Aerospace Engineering and Engineering Mechanics. Fellow AIAA.

‡Research Scientist, Integrated Systems Technologies Branch. Member AIAA.

The prime in the preceding equations indicates that the streamwise (ξ direction) viscous terms have been dropped. These same viscous terms are also dropped in the thin-layer NS equations and the boundary-layer equations. The inviscid (subscript i) and viscous (subscript v) flux vectors are given by

$$\boldsymbol{E}_i = \left\{\rho u, \rho u^2 + p, \rho uv, \rho uw, (E_t + p)u\right\}^T$$

$$\boldsymbol{F}_i = \left\{\rho v, \rho uv, \rho v^2 + p, \rho vw, (E_t + p)v\right\}^T$$

$$\boldsymbol{G}_i = \left\{\rho w, \rho uw, \rho vw, \rho w^2 + p, (E_t + p)w\right\}^T$$

$$\boldsymbol{E}_v = \{0, \tau_{xx}, \tau_{xy}, \tau_{xz}, u\tau_{xx} + v\tau_{xy} + w\tau_{xz} - q_x\}^T$$

$$\boldsymbol{F}_v = \{0, \tau_{yx}, \tau_{yy}, \tau_{yz}, u\tau_{yx} + v\tau_{yy} + w\tau_{yz} - q_y\}^T$$

$$\boldsymbol{G}_v = \{0, \tau_{zx}, \tau_{zy}, \tau_{zz}, u\tau_{zx} + v\tau_{zy} + w\tau_{zz} - q_z\}^T$$

where $E_t = \rho\{e + \frac{1}{2}(u^2 + v^2 + w^2)\}$. In the present study, the coefficient of viscosity is calculated by the use of Sutherland's equation and the coefficient of thermal conductivity is computed under the assumption of a constant Prandtl number. Finally, the system is closed by the use of the perfect gas equation of state.

The PNS equations are a mixed set of hyperbolic–parabolic equations in the streamwise direction provided that the inviscid flow is supersonic, the streamwise velocity component is everywhere greater than zero, and the streamwise pressure gradient term is either omitted in subsonic regions or the departure behavior is suppressed. Vigneron et al.[15] have shown that the PNS equations will remain hyperbolic–parabolic in subsonic (unseparated) regions if only a fraction ω of the streamwise pressure gradient is retained. The fraction ω is given by

$$\omega = \min\left[1, \frac{\beta\gamma M_\xi^2}{1 + (\gamma - 1)M_\xi^2}\right] \tag{3}$$

where M_ξ is the local Mach number in the ξ direction and β is a safety factor that accounts for nonlinearities in the analysis. Upon incorporating Vigneron's technique into the three-dimensional PNS equations, the $\boldsymbol{E}$ vector becomes

$$\boldsymbol{E} = \boldsymbol{E}^* + \boldsymbol{E}^p \tag{4}$$

where

$$\boldsymbol{E}^* = \frac{\xi_x}{J}\begin{bmatrix}\rho u\\ \rho u^2 + \omega p\\ \rho uv\\ \rho uw\\ (E_t + p)u\end{bmatrix} + \frac{\xi_y}{J}\begin{bmatrix}\rho v\\ \rho uv\\ \rho v^2 + \omega p\\ \rho vw\\ (E_t + p)v\end{bmatrix} + \frac{\xi_z}{J}\begin{bmatrix}\rho w\\ \rho uw\\ \rho vw\\ \rho w^2 + \omega p\\ (E_t + p)w\end{bmatrix} \tag{5}$$

$$\boldsymbol{E}^p = \frac{\xi_x}{J}\begin{bmatrix}0\\ (1 - \omega)p\\ 0\\ 0\\ 0\end{bmatrix} + \frac{\xi_y}{J}\begin{bmatrix}0\\ 0\\ (1 - \omega)p\\ 0\\ 0\end{bmatrix} + \frac{\xi_z}{J}\begin{bmatrix}0\\ 0\\ 0\\ (1 - \omega)p\\ 0\end{bmatrix} \tag{6}$$

The elliptic portion ($\boldsymbol{E}^p$) of the streamwise pressure gradient is omitted in the subsonic portion of the flowfield when using a standard single-sweep PNS code. Note that the three-dimensional PNS equations are elliptic in each crossflow plane and the equations are solved simultaneously at every cell in the plane. Thus, any upstream effects occurring in the crossflow plane are automatically calculated.

Iterated PNS Algorithm

Several investigators[16–26] have extended the single-sweep PNS method to permit the computation of flows where upstream influence effects are important. In all of these previous studies, the iterative procedure is either performed throughout the entire flowfield or in a region that is defined before the computation of the flowfield. In those methods where the iterative procedure is performed within only a portion of the flowfield, the boundaries of the embedded region are often defined by the use of detailed prior knowledge of the flowfield being computed. In the present study, a technique is presented that permits the boundaries of the embedded region to be located automatically before the calculation of the flowfield. This technique is described in the next section.

One of the first attempts to modify the single-sweep PNS method to compute flows with upstream influences was described by Rakich[16] in 1983. In his approach, the pressure gradient is split by the use of the technique of Vigneron et al.[15] A mechanism for the incorporation of upstream influence effects is provided by the use of a forward difference for $\partial\boldsymbol{E}^p/\partial\xi$. The present iterative PNS (IPNS) algorithm is based in part on the methods of Rakich,[16] Barnett and Davis,[19] and Power.[25] The algorithm is first-order accurate in the streamwise direction and the number of iterations required for convergence is comparable to the number of streamwise points in the embedded region. The convergence rate can be accelerated by the use of the method of Barnett and Davis.[19]

Flux Differencing

The details of the streamwise flux differencing employed in the IPNS algorithm are given here using a finite volume formulation. The streamwise flux vectors $\boldsymbol{E}^*$ and $\boldsymbol{E}^p$ are functions of the metrics, that is, geometry, designated by $d\boldsymbol{S}_i$ and the conserved flow variables $\boldsymbol{U}$ where $\boldsymbol{U} = [\rho, \rho u, \rho v, \rho w, E_t]^T$. It is convenient to represent the flux vectors at a given station ξ by the use of the functional notation

$$\boldsymbol{E}^*_{i+1} = \boldsymbol{E}^*(d\boldsymbol{S}_{i+1}, \boldsymbol{U}_{i+1}), \qquad \boldsymbol{E}^p_{i+1} = \boldsymbol{E}^p(d\boldsymbol{S}_{i+1}, \boldsymbol{U}_{i+1}) \tag{7}$$

where the subscript $i + 1$ denotes the spatial index (in the ξ direction) where the solution is currently being computed. In a manner similar to Rakich,[16] the IPNS method is derived by the use of a forward difference for the elliptic portion of the streamwise gradient so that the complete expression for the streamwise gradient becomes

$$\left(\frac{\partial\boldsymbol{E}}{\partial\xi}\right)_{i+1} = \frac{1}{\Delta\xi}\Big[\boldsymbol{E}^*_{i+1} - \boldsymbol{E}^*_i + \boldsymbol{E}^p(d\boldsymbol{S}_{i+1}, \boldsymbol{U}_{i+2}) - \boldsymbol{E}^p(d\boldsymbol{S}_i, \boldsymbol{U}_{i+1})\Big] \tag{8}$$

where $\boldsymbol{U}_{i+2}$ is obtained from the preceding sweep. This expression is a finite volume representation of the streamwise gradient and is first-order accurate in the streamwise direction. The $\boldsymbol{E}^*$ and the $\boldsymbol{E}^p$ terms evaluated at the $i + 1$ and $i + 2$ stations are linearized as follows:

$$\boldsymbol{E}^*_{i+1} = \boldsymbol{E}^*(d\boldsymbol{S}_{i+1}, \boldsymbol{U}_i) + A^*(d\boldsymbol{S}_{i+1}, \boldsymbol{U}_i)\Delta\boldsymbol{U}_i$$

$$\boldsymbol{E}^p(d\boldsymbol{S}_i, \boldsymbol{U}_{i+1}) = \boldsymbol{E}^p_i + A^p_i\Delta\boldsymbol{U}_i$$

$$\boldsymbol{E}^p(d\boldsymbol{S}_{i+1}, \boldsymbol{U}_{i+2}) = \boldsymbol{E}^p(d\boldsymbol{S}_{i+1}, \boldsymbol{U}_i) + A^p_{i+1}[\boldsymbol{U}_{i+2} - \boldsymbol{U}_i] \tag{9}$$

where $\Delta\boldsymbol{U}_i = \boldsymbol{U}_{i+1} - \boldsymbol{U}_i$ and the Jacobians are defined by

$$A^*(d\boldsymbol{S}_{i+1}, \boldsymbol{U}_i) = \frac{\partial\boldsymbol{E}^*(d\boldsymbol{S}_{i+1}, \boldsymbol{U}_i)}{\partial\boldsymbol{U}_i}$$

$$A^p_i = A^p(d\boldsymbol{S}_i, \boldsymbol{U}_i) = \frac{\partial\boldsymbol{E}^p(d\boldsymbol{S}_i, \boldsymbol{U}_i)}{\partial\boldsymbol{U}_i}$$

By substitution of the identities

$$\boldsymbol{E}_i^* = A_i^* \boldsymbol{U}_i, \qquad \boldsymbol{E}^*(d\boldsymbol{S}_{i+1}, \boldsymbol{U}_i) = A^*(d\boldsymbol{S}_{i+1}, \boldsymbol{U}_i)\boldsymbol{U}_i$$
$$\boldsymbol{E}_i^p = A_i^p \boldsymbol{U}_i, \qquad \boldsymbol{E}^p(d\boldsymbol{S}_{i+1}, \boldsymbol{U}_i) = A^p(d\boldsymbol{S}_{i+1}, \boldsymbol{U}_i)\boldsymbol{U}_i \quad (10)$$

and the linearizations given by Eq. (9), the expression for the streamwise gradient of $\boldsymbol{E}$ becomes

$$\left(\frac{\partial \boldsymbol{E}}{\partial \xi}\right)_{i+1} = \frac{1}{\Delta \xi}\left\{\left[A^*(d\boldsymbol{S}_{i+1}, \boldsymbol{U}_i) - A_i^p\right]\Delta \boldsymbol{U}_i + [A(d\boldsymbol{S}_{i+1}, \boldsymbol{U}_i) - A_i]\boldsymbol{U}_i + A_{i+1}^p[\boldsymbol{U}_{i+2} - \boldsymbol{U}_i]\right\} \quad (11)$$

where $A = A^* + A^p$. To simplify the computation of the explicit portion of the preceding equation, the last term is replaced with the following approximation, which does not change the overall accuracy of the method:

$$A_{i+1}^p[\boldsymbol{U}_{i+2} - \boldsymbol{U}_i] \cong \boldsymbol{E}^p(d\boldsymbol{S}_{i+1}, \boldsymbol{U}_{i+2}) - \boldsymbol{E}^p(d\boldsymbol{S}_{i+1}, \boldsymbol{U}_i) \quad (12)$$

The final discretized form of the equations used in the IPNS approach is obtained by substitution of Eqs. (11) and (12) into Eq. (1) along with the linearized expressions for the fluxes in the crossflow plane. In three dimensions, the final expression becomes

$$\left\{\frac{1}{\Delta \xi}\left[A^*(d\boldsymbol{S}_{i+1}, \boldsymbol{U}_i) - A_i^p\right]^{k+1} + \frac{\partial}{\partial \eta}\left[\frac{\partial \boldsymbol{F}(d\boldsymbol{S}_{i+1}, \boldsymbol{U}_i)}{\partial \boldsymbol{U}}\right]^{k+1} + \frac{\partial}{\partial \zeta}\left[\frac{\partial \boldsymbol{G}(d\boldsymbol{S}_{i+1}, \boldsymbol{U}_i)}{\partial \boldsymbol{U}}\right]^{k+1}\right\}\Delta \boldsymbol{U}_i^{k+1} = \text{RHS}$$

where RHS indicates right-hand side and is given by

$$\text{RHS} = -\frac{1}{\Delta \xi}\left\{[A(d\boldsymbol{S}_{i+1}, \boldsymbol{U}_i) - A_i]^{k+1}\boldsymbol{U}_i^{k+1} - \boldsymbol{E}^p(d\boldsymbol{S}_{i+1}, \boldsymbol{U}_{i+2})^k + \boldsymbol{E}^p(d\boldsymbol{S}_{i+1}, \boldsymbol{U}_i)^{k+1}\right\} - \left[\frac{\partial \boldsymbol{F}(d\boldsymbol{S}_{i+1}, \boldsymbol{U}_i)}{\partial \eta}\right]^{k+1} - \left[\frac{\partial \boldsymbol{G}(d\boldsymbol{S}_{i+1}, \boldsymbol{U}_i)}{\partial \zeta}\right]^{k+1} \quad (13)$$

and the superscript $k+1$ denotes the current iteration level. Further details of the IPNS algorithm are given in Refs. 27 and 28.

Separated Flows

Special treatment is required for separated flows because the streamwise component of velocity becomes negative and the convective fluxes are in a direction that is opposite to the marching direction. To overcome this difficulty, the FLARE approximation[29] is used in separated regions. This is accomplished by our setting any negative streamwise velocity components that occur in the coefficients of convective terms to zero or a very small positive number. Also for separated flows, the governing equations are elliptic and, therefore, ω is set to zero in the region from the wall to the edge of the boundary layer and is set to one above the boundary layer. This is consistent with the work of Power[25] where the line of influence was used to include displacement effects.

For flows with very large separated regions, the IPNS method will fail because of the FLARE approximation. For these cases, another approach has been developed by the present authors[30,31] that utilizes the Steger–Warming flux splitting in place of the original Vigneron splitting (see Ref. 15). This eliminates the need for the FLARE approximation and also does not require the specification of the boundary layer edge for ω.

Downstream Boundary Condition

The expression for the streamwise gradient [Eq. (11)] requires information from a point downstream of the IPNS region when we compute the last station in the IPNS region. Several approaches have been used previously to implement this boundary condition for iterative PNS methods. In the present study, the gradient is assumed to be locally linear and the exterior point is updated after every sweep, with the gradient set equal to the gradient computed from the preceding sweep.

Marching Procedure

The flowfields considered in this study include only those where a single-sweep PNS solution is obtainable, but the solution may not be accurate. Included are flowfields where the interaction between the inviscid and viscous portions of the flow is significant and may produce an embedded separated region. If the flowfield meets these requirements, then the present approach to the problem can be described as follows. First, the standard PNS solver is employed until the beginning of the interaction region is reached. The standard PNS algorithm is then used to obtain the initial solution in the embedded region. As this initial solution is being computed, the pressure is stored at every station in the embedded region. After completing the first sweep, the process is repeated, but now the streamwise gradient is differenced as described earlier to include downstream effects. The process is continued until the specified convergence criterion is met. After a converged solution is obtained in the embedded region, the standard single-sweep PNS method is resumed until the next embedded region is encountered.

UPS Code

The new IPNS algorithm has been successfully incorporated into the UPS code originally developed by Lawrence et al.[13,14] The UPS code solves the parabolized NS equations by the use of a fully conservative, finite volume approach in a general nonorthogonal coordinate system. The UPS code was originally developed for perfect gas flows and uses an upwind, total variation diminishing (TVD) method based on Roe's approximate Riemann solver.[32] During the last several years, the code has been modified to permit the accurate calculation of many types of flows, including those in thermochemical nonequilibrium.

Detection of Regions That Cause Upstream Influence

To compute successfully the entire flowfield surrounding a supersonic/hypersonic vehicle using a PNS code, it is necessary to detect and measure the extent of embedded regions that produce significant upstream effects. In the present approach, the body geometry is scanned before the flowfield is computed and the lengths of the embedded regions are computed by the use of the correlation functions discussed hereafter. This method has been incorporated into the UPS code so that the detection process is completely automated with the flowfield computation.

The correlation functions developed in this study for two-dimensional laminar flows were determined by empirical methods because of the lack of accurate theoretical or experimental relations that could be used for the determination of the lengths of the embedded regions. Correlation functions were obtained for compression ramp, expansion corner, and shock impingement flowfields. These functions are the first correlations (theoretical or empirical) to predict accurately where the single-sweep PNS method is inaccurate for a range of flow conditions.

The present correlation functions accurately predict the ratio of the upstream influence distance l_u to the boundary-layer thickness δ_L. The ratio l_u/δ_L is often used in theoretical studies of separated laminar flows. The downstream influence distance is given by l_d. Definitions of the various lengths are shown in Fig. 1 for the case of flow over a compression ramp. The distance L is defined as the length measured from the leading edge to the source of the disturbance. In the case of an impinging shock, L is the location of the impingement point, and, for an expansion corner, L is the location of the corner.

The quantity δ_L is defined as the boundary-layer thickness of the undisturbed flow at the x (or ξ) station L. An empirical formula for the boundary-layer thickness is given by White[33]:

$$\delta = x\sqrt{C_w}/\sqrt{Re_x}\left\{5.0 + [0.2 + 0.9(T_w/T_{aw})](\gamma - 1)M_\infty^2\right\} \quad (14)$$

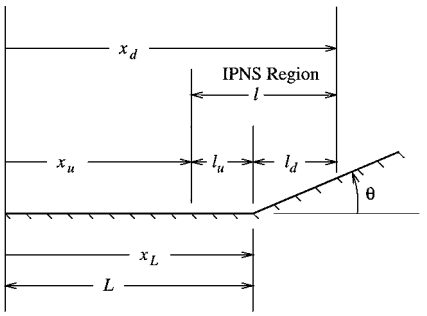

Fig. 1 Location and length definitions for detection of embedded regions.

where

$$C_w = \rho_w \mu_w / \rho_\infty \mu_\infty \cong (T_w / T_\infty)^{-\frac{1}{3}} \tag{15}$$

$$T_{aw} = T_\infty \left\{ 1 + [(\gamma - 1)/2] \sqrt{Pr} M_\infty^2 \right\} \tag{16}$$

Based on dimensional analysis, it is assumed that the extent of the embedded region is dependent upon four nondimensional quantities provided that the Prandtl number and γ are fixed. These four quantities are Mach number M, Reynolds number Re, wall temperature ratio T_w / T_{aw}, and the relative pressure change in the inviscid flow $\Delta p / p_{\text{ref}}$, where p_{ref} is a reference pressure. The relative change in pressure for an inviscid flow is easily determined for simple geometries if the freestream Mach number is known.[34] In addition, this study is limited to an adiabatic wall condition so that the ratio T_w / T_{aw} is assumed to be equal to one.

Because the IPNS algorithm is able to compute solutions accurately over a range of flow conditions, it was used to generate the data needed for the determination of the empirical correlations. Flowfields involving two-dimensional compression ramps (25 cases), expansion corners (45 cases), and shock impingements (20 cases) were computed, and these results are given in Refs. 27 and 28. The computed (grid-independent) results were used to determine the exponents and constants in the correlations. The data obtained from the numerical study covered a Mach number range from 2.0 to 6.06, with the majority of data between 2.0 and 3.0. The range of Reynolds numbers was from 1×10^4 to 8×10^5. The beginning of the interaction region was defined as the location where the skin friction coefficient differed from the computed undisturbed flat-plate value by 1%.

The downstream boundary of the interaction region was determined in a more approximate way. For the compression ramp and shock impingement flowfields, the location of the downstream boundary was determined by the examination of the skin-friction coefficient as a function of x. A relatively constant value of skin-friction coefficient was used to define the end of the embedded region. For the expansion corner flowfields, several computations were performed for each set of freestream conditions and angle geometry (25 cases). The value of l_d was chosen so that the computed skin-friction coefficient was nearly continuous between the IPNS and PNS solutions at the downstream boundary.

The correlation functions were determined from a least-squares statistical analysis of the computed data. The total length of the embedded region l was chosen to be a linear function of l_u for ramp and shock impingement flowfields:

$$l = K l_u \tag{17}$$

where K is a constant. The constants determined for ramp flowfields and shock impingement flowfields were 2.6 and 2.3, respectively. To account for the approximations made in the analysis, the correlation functions are written with an additional safety factor σ. Numerical experimentation indicates that a value of $\sigma \cong 1.0 - 1.2$ is sufficient. The final forms of the correlation functions are given for compression ramp flowfields:

$$l_u / \delta_L = \sigma (\Delta p / p_\infty)^{\frac{3}{8}} \left(Re_L^{\frac{3}{8}} \Big/ M_\infty^{\frac{3}{2}} \right) \tag{18}$$

$$l = 2.6 l_u \tag{19}$$

for shock impingement flowfields:

$$l_u / \delta_L = \sigma \tfrac{1}{2} (\Delta p / p_\infty)^{\frac{1}{5}} \left(Re_L^{\frac{2}{5}} \Big/ M_\infty \right) \tag{20}$$

$$l = 2.3 l_u \tag{21}$$

and for expansion corner flowfields:

$$l_u / \delta_L = \sigma \tfrac{1}{6} (|\Delta p| / p_\infty)^{\frac{1}{10}} \left[\left(Re_L^{\frac{2}{5}} \Big/ M_\infty \right) + 15 \right] \tag{22}$$

$$l_d / \delta_L = \sigma \tfrac{1}{15} (|\Delta p| / p_d)^{\frac{1}{4}} Re_L^{\frac{1}{2}} \tag{23}$$

where p_d is the pressure downstream of the corner.

The upstream influence correlation functions are plotted in Figs. 2–4 along with the numerical and experimental data[35–41] for the compression ramp, shock impingement, and expansion corner cases, respectively. It is clear that the correlation functions accurately predict the upstream influence over a range of flow conditions. The scatter in the experimental data with the correlation functions is due to the difficulty in interpreting the experimental data from graphs presented by the authors as well as other factors that are associated with performing experiments in general. The downstream influence functions are plotted in Refs. 27 and 28.

Numerical Results

The new iterative parabolized NS code developed in this study has been used to compute several two-dimensional laminar flow test cases. All of these test cases include embedded regions that produce significant upstream effects. The lengths of the embedded regions were automatically determined before the flowfield computations. Further details of these calculations are given in Refs. 27 and 28.

Test Case 1

Figure 1 shows the geometry for the first test case, which consists of a flat plate followed by a 10-deg compression ramp. The freestream Mach number is 3.0, and the Reynolds number based on the length of the flat plate region ($L = 1.0$ m) is 1.68×10^4. The wall temperature and freestream temperature are 606.7 and 216.7 K, respectively. These flow conditions correspond to the test case originally computed by Carter[42] using the complete NS equations. The flow in this case is separated and the ramp induces significant upstream effects.

The finest grid used for this case (to ensure grid independence) consisted of 90 points in the normal direction and 309 in the streamwise direction with 200 streamwise points in the IPNS region ($0.5 < x < 1.8$ m). Figures 5 and 6 show the computed wall pressure and skin friction, respectively. Also shown are the NS results of Hung and MacCormack[43] and the computed PNS results. The agreement between the IPNS results and the NS approach is excellent. The skin-friction coefficient is defined as

$$C_f = \left. \frac{\mu}{\frac{1}{2} \rho_\infty V_\infty^2} \frac{\partial u}{\partial n} \right|_{\text{wall}} \tag{24}$$

where n is in a direction normal to the body surface.

A grid refinement study was performed, and the results[27] indicate that grid independence has been achieved. Figure 7 shows the pressure convergence history based on the rms of the relative change in pressure in the IPNS region. The rms is defined as

$$\text{rms} = \sqrt{\frac{1}{j_{\max}} \sum_{j=1}^{j=j_{\max}} \left(\frac{p_j^{k+1} - p_j^k}{p_j^k} \right)^2} \tag{25}$$

where the summation is over all points ($j = 1, 2, \ldots j_{\max}$) in the IPNS region where $\omega < 1$. The number of streamwise sweeps required for convergence on the finest grid was 166. For this study, the calculations are considered to be converged when the rms value is less than 10^{-4}.

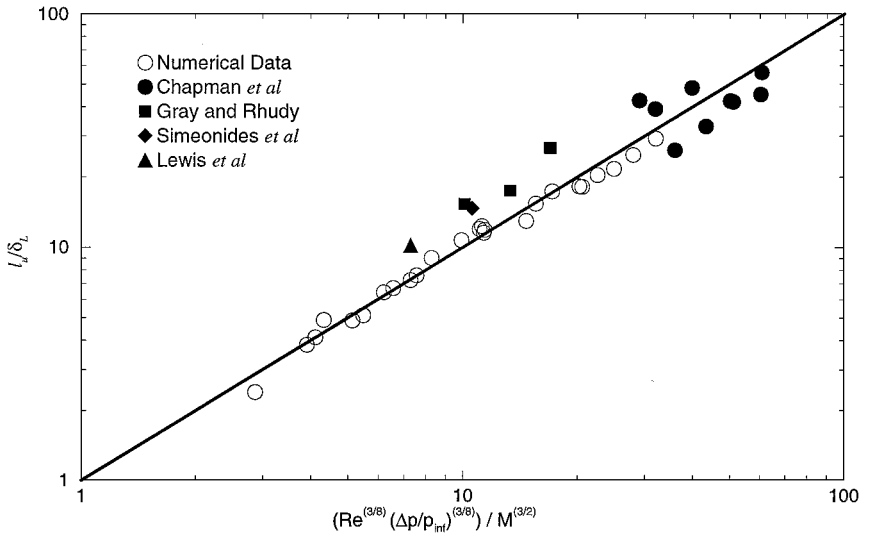

Fig. 2 Correlation function l_u for compression ramp flowfields.

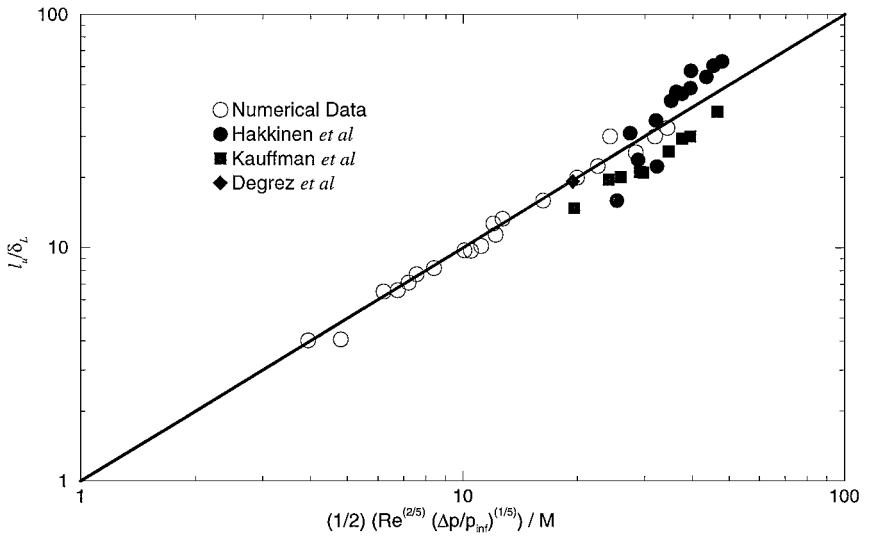

Fig. 3 Correlation function l_u for shock impingement flowfields.

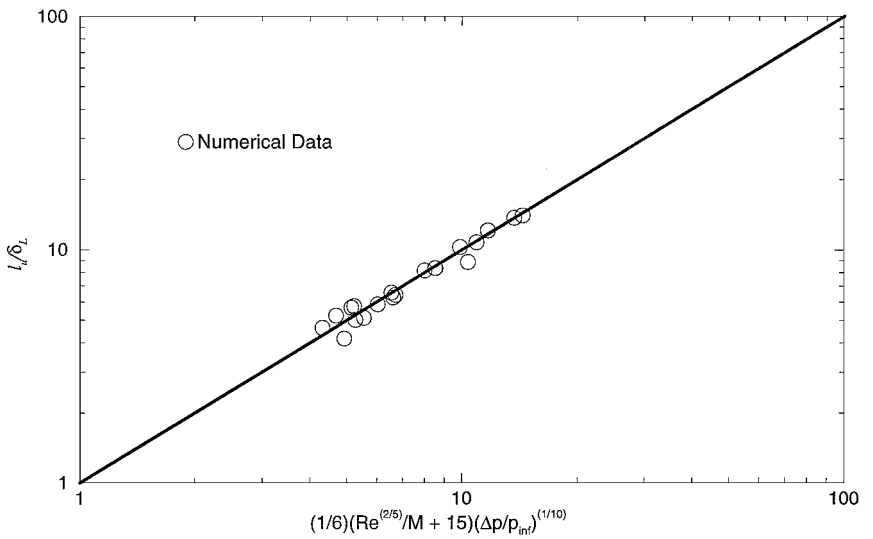

Fig. 4 Correlation function l_u for expansion corner flowfields.

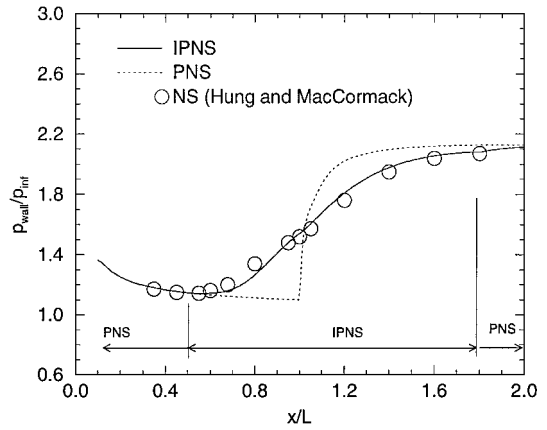

Fig. 5 Wall pressure results for 10-deg ramp.

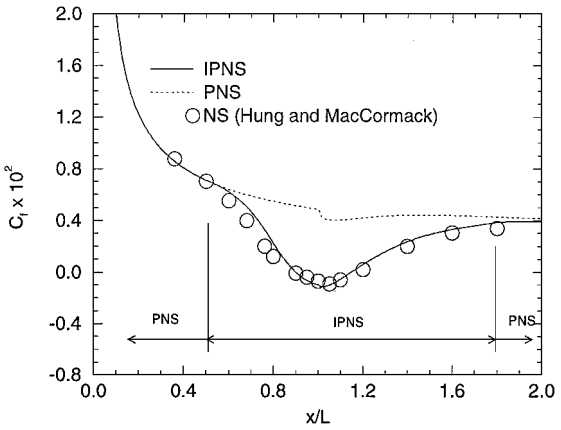

Fig. 6 Skin-friction results for 10-deg ramp.

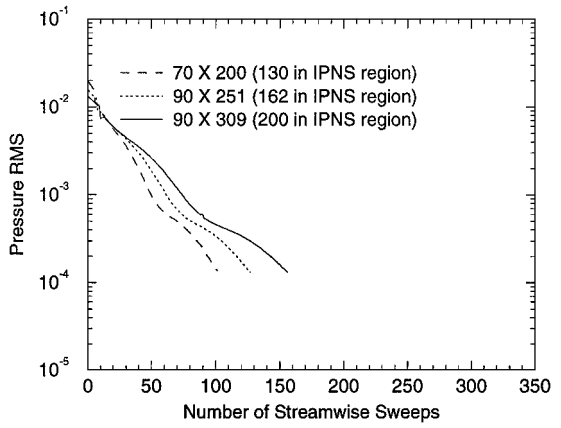

Fig. 7 Pressure rms histories.

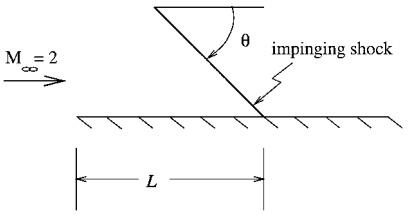

Fig. 8 Shock impingement geometry.

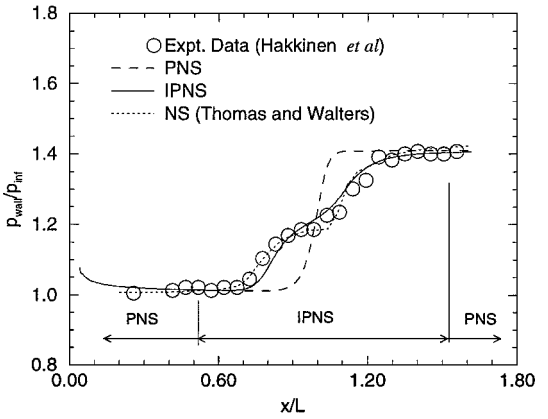

Fig. 9 Wall pressure results.

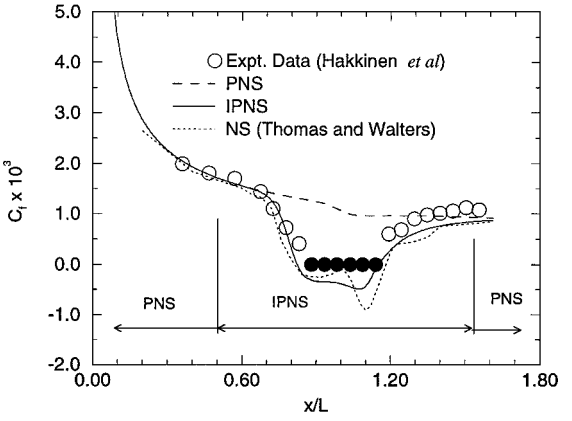

Fig. 10 Skin-friction results.

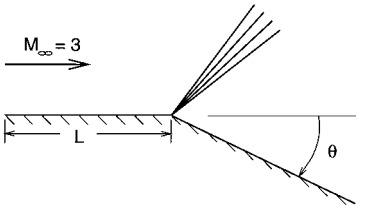

Fig. 11 Expansion corner geometry.

Test Case 2

The second test case consists of an oblique shock impinging on a laminar boundary layer that is developing on a flat plate. The geometry is shown in Fig. 8. This case corresponds to the experiment performed by Hakkinen et al.[39] The freestream Mach number is 2.0, and the Reynolds number based on the location of the shock impingement point ($L = 0.049$ m) is 2.96×10^5. The shock angle (θ) is 32.6 deg, and the plate is modeled with an adiabatic wall boundary condition.

The finest grid used for this case consisted of 170 points in the normal direction and 415 in the streamwise direction, with 250 points in the IPNS region ($0.025 < x < 0.075$ m). The first point above the wall was located at 1×10^{-5} m. These results are considered to be grid independent. The number of streamwise sweeps required for convergence on the finest grid was 267.

The wall pressure and skin-friction results are shown in Figs. 9 and 10, respectively. Also shown are the NS results computed by Thomas and Walters[44] and the PNS results. The solid symbols in Fig. 10 indicate where separated flow was detected by Hakkinen et al.[39] but the skin friction was not measured. The IPNS results are in good agreement with the NS results and experimental data. Note that the present case contains a significant region of separated flow and that the FLARE approximation does affect the details of the separation, as seen in Figs. 9 and 10. However, the extent of the separation region is in excellent agreement with the NS results and experimental data.

Test Case 3

Figure 11 shows the geometry for the third test case, which consists of a flat plate followed by a 25-deg expansion corner. The

freestream Mach number is 3.0, and the Reynolds number based on the length of the flat-plate region ($L = 1.0$ m) is 1.68×10^4. The wall temperature and freestream temperature are 547.6 and 216.67 K, respectively. The flow in this case is not separated but the expansion ramp induces significant upstream effects.

The finest grid used for this case (to ensure grid independence) consisted of 120 points in the normal direction and 245 in the streamwise direction with 112 streamwise points in the IPNS region ($0.66 < x < 2.0$ m). The computed wall pressure and skin friction are shown in Figs. 12 and 13, respectively, along with the results computed with the NS code OVERFLOW[45] and the results obtained by the use of the standard PNS approach. The agreement between the IPNS and NS results is excellent. The PNS results were obtained by the use of the same grid as the IPNS solution. The grid used for the OVERFLOW code was the same except for 10 streamwise points added to the leading edge of the plate. A grid refinement study was performed, and the results[28] indicate that grid independence has been achieved. The number of streamwise sweeps required for convergence on the finest grid was 35.

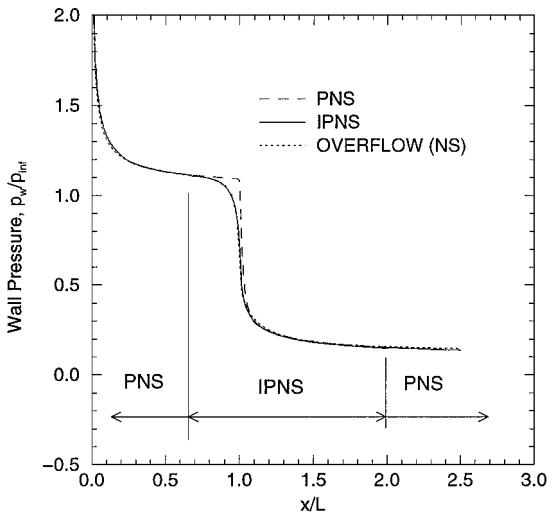

Fig. 12 Wall pressure results for 25-deg expansion.

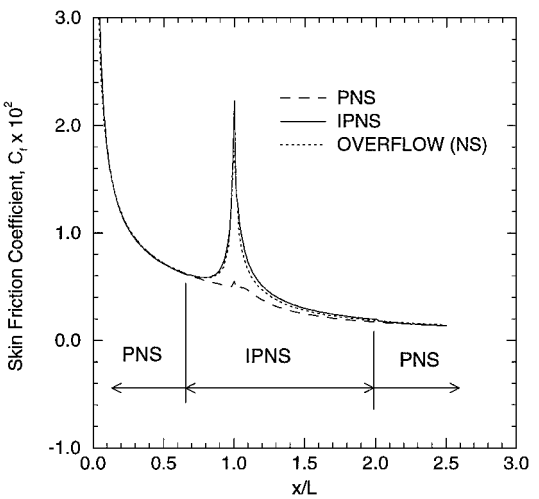

Fig. 13 Skin-friction results for 25-deg expansion.

To demonstrate the computational efficiency of the current approach, a grid refinement study was also performed with the NS code OVERFLOW. The OVERFLOW code required the same number of grid points as the IPNS code to achieve grid independence. The results of the OVERFLOW grid refinement study are given in Ref. 46. The required CPU times and memory are listed in Table 1. Note that the current method requires at least an order of magnitude less computer time and much less memory than the OVERFLOW code for each of the grids used. The computational effort is obviously problem dependent; however, these results demonstrate the significant savings that can be achieved with the current approach.

Test Case 4

The fourth test case involves a more complicated geometry that produces two regions where upstream effects are important. The geometry consists of a 15-deg wedge followed by a flat plate region and then a 7-deg ramp. The geometry is shown in Fig. 14. The ramp induces a significant separated region. The lengths of the IPNS regions were automatically computed before the flowfield calculation by scanning the geometry and using the appropriate correlation functions with the inviscid flow conditions and a safety factor σ of 1.1. See Ref. 47 for further details. The IPNS regions are shown in Fig. 15.

The flow conditions are a Mach number of 3.0, a Reynolds number (based on the total length $L = 35.0$ m) of 1.47×10^5, a freestream temperature of 216.67 K, and a wall temperature of 547.6 K. The wall temperature was chosen to be equal to the adiabatic wall temperature for the given Mach number and a Prandtl number of 0.72.

The computed wall pressure and skin friction are shown in Figs. 16 and 17, respectively, along with the results obtained by the use of the standard PNS approach and the NS approach using the OVERFLOW code. The PNS results were obtained by the use of the same grid as the IPNS solution, whereas the OVERFLOW solution was obtained by the use of the same grid but with 10 streamwise points added at the leading edge of the geometry. The agreement between the IPNS method and the OVERFLOW code is excellent. The small difference in results near the leading edge is believed to be due to the grids used at the leading-edge singularity. Note that the standard single-sweep PNS approach is noticeably inaccurate in terms of the streamwise variation of skin friction and wall pressure.

A grid refinement study was performed,[28] and the results indicate that grid independence has been achieved. The finest grid utilized 40 points in the first IPNS region ($2.61 < x < 5.80$ m) and 206 in the second IPNS region ($13.56 < x < 30.03$ m). The CPU time on a DEC Alphastation 255 for the OVERFLOW code (70×505) was 2000.0 s, whereas the time required by the IPNS code (70×497) was 455.0 s. In addition, three different safety factors ($\sigma = 1.0$, 1.1, and 1.2) were used to determine the lengths of the IPNS regions and the computed results indicate negligible differences for the three safety factors considered. It was also found that the rates of convergence

Table 1 Required CPU times and memory for test case 3

	CPU time, s		Memory, MB	
Grid	OVERFLOW	IPNS	OVERFLOW	IPNS
$70 \times 161(151)$	253.5	12.6	7.0	3.3
$120 \times 192(182)$	725.6	43.6	13.0	4.6
$120 \times 255(245)$	914.6	82.0	17.0	4.8

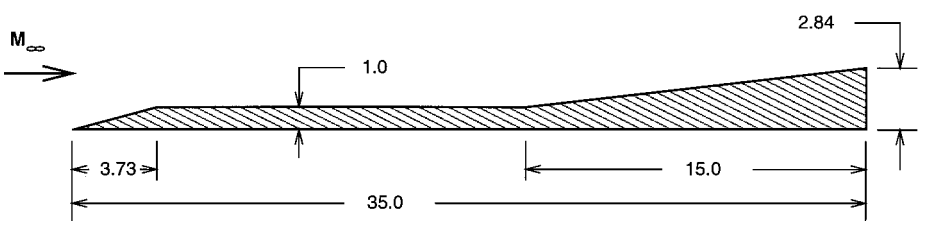

Fig. 14 Geometry for multiple-embedded-region case.

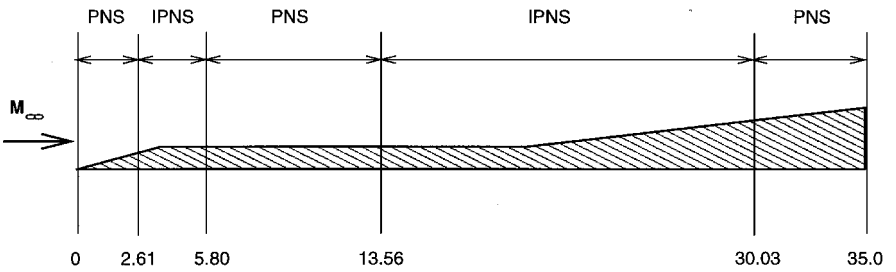

Fig. 15 IPNS regions for multiple-embedded-region case.

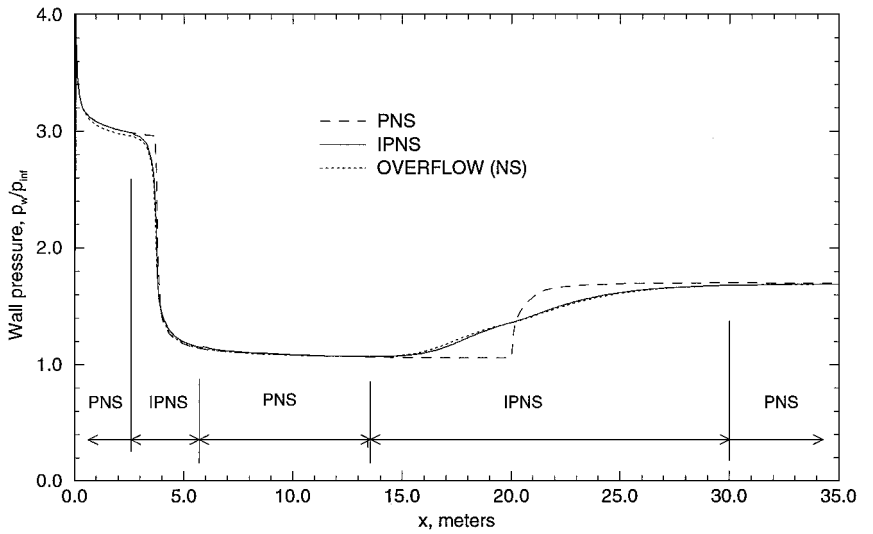

Fig. 16 Wall pressure results for multiple-embedded-region geometry.

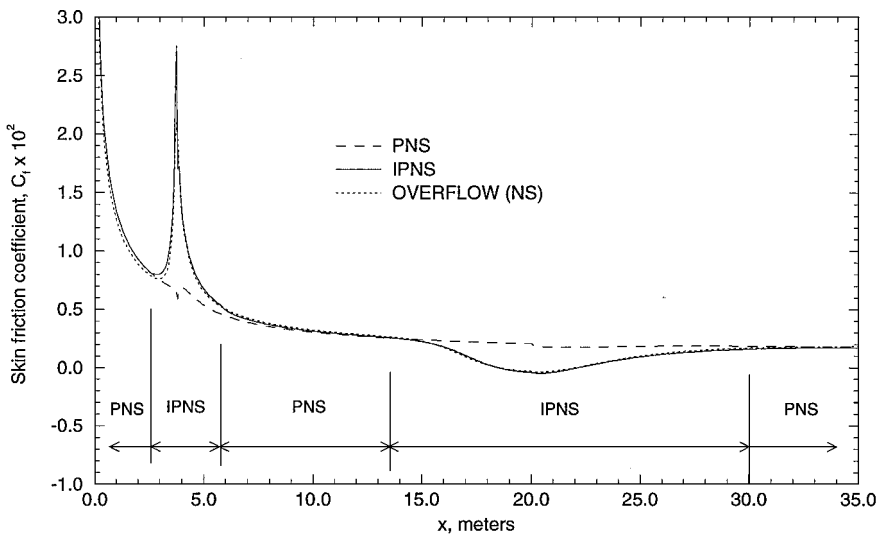

Fig. 17 Skin-friction results for multiple-embedded-region geometry.

for these computations were not significantly affected by the choice of safety factor.

Summary

A new PNS algorithm has been developed that significantly reduces the computer time and storage required to calculate supersonic flows with embedded regions that produce upstream effects. The algorithm has been applied to several test cases and the computed results are in excellent agreement with NS computations and experimental data. Work has recently been completed on extending the present approach to arbitrary shapes including curved surfaces. These arbitrary shapes are first decomposed into a series of very small compression ramps, expansion corners, or flat surfaces, thereby permitting the use of the correlation functions to predict the lengths of the corresponding upstream and downstream influence regions.

Acknowledgments

This work was supported by NASA Ames Research Center through Small Business Innovative Research Contract NAS2-14327. The technical monitor for this contract was Scott Lawrence. In addition, this work was supported in part by The Boeing Company through a Research Fellowship. The authors wish to thank Pieter Buning for his assistance with the OVERFLOW code and Alric Rothmayer for discussions related to this work.

References

[1]Tannehill, J. C., Anderson, D. A., and Pletcher, R. H., *Computational Fluid Mechanics and Heat Transfer*, 2nd ed., Taylor and Francis, Washington, DC, 1997, pp. 545–584.

[2]Rubin, S. G., and Tannehill, J. C., "Parabolized/Reduced Navier–Stokes Computational Techniques," *Annual Review of Fluid Mechanics*, Vol. 24, 1992, pp. 117–144.

[3]Wood, W. A., and Thompson, R. A., "Combined LAURA-UPS Hypersonic Solution Procedure," NASA TM-107682, March 1993.

[4]Lombard, C. K., Venkatapathy, E., and Bardina, J., "Universal Single Level Implicit Algorithm for Gas Dynamics," AIAA Paper 84-1533, 1984.

[5]Newsome, R. W., Walters, R. W., and Thomas, J. L., "An Efficient Iteration Strategy for Upwind/Relaxation Solutions to the Thin-Layer Navier–Stokes Equations," AIAA Paper 87-1113, June 1987.

[6]Ota, D. K., Chakravarthy, S. R., and Darling, J. C., "An Equilibrium Air Navier–Stokes Code for Hypersonic Flows," AIAA Paper 88-0419, 1988.

[7]Molvik, G. A., and Merkle, C. L., "A Set of Strongly Coupled, Upwind Algorithms for Computing Flows in Chemical Nonequilibrium," AIAA Paper 89-0199, 1989.

[8]Chang, C. L., and Merkle, C. L., "The Relation Between Flux Vector Splitting and Parabolized Schemes," *Journal of Computational Physics*, Vol. 80, No. 1, 1989, pp. 344–361.

[9]Matus, R. J., and Bender, E. E., "Application of a Direct Solver for Space Marching Solutions," AIAA Paper 90-1442, 1990.

[10]Greene, F. A., "An Upwind-Biased Space Marching Algorithm for Supersonic Viscous Flow," NASA TP-3068, March 1991.

[11]Nakahashi, K., and Saitoh, E., "Space-Marching Method on Unstructured Grid for Supersonic Flows with Embedded Subsonic Regions," AIAA Paper 96-0418, Jan. 1996.

[12]Buelow, P. E., Ievalts, J. O., and Tannehill, J. C., "Comparison of Three-Dimensional Nonequilibrium PNS Codes," AIAA Paper 90-1572, June 1990.

[13]Lawrence, S. L., Tannehill, J. C., and Chaussee, D. S., "Upwind Algorithm for the Parabolized Navier–Stokes Equations," *AIAA Journal*, Vol. 27, No. 9, 1989, pp. 1175–1183.

[14]Lawrence, S. L., Chaussee, D. S., and Tannehill, J. C., "Application of an Upwind Algorithm to the Three-Dimensional Parabolized Navier–Stokes Equations," *AIAA Journal*, Vol. 28, No. 6, 1990, pp. 971, 972.

[15]Vigneron, Y. C., Rakich, J. V., and Tannehill, J. C., "Calculation of Supersonic Flow over Delta Wings with Sharp Subsonic Leading Edges," AIAA Paper 78-1137, July 1978.

[16]Rakich, J. V., "Iterative PNS Method for Attached Flows with Upstream Influence," AIAA Paper 83-1955, July 1983.

[17]Rubin, S. G., and Reddy, D. R., "Analysis of Global Pressure Relaxation for Flows with Strong Interaction and Separation," *Computers and Fluids*, Vol. 11, No. 4, 1983, pp. 281–306.

[18]Khosla, P. K., and Lai, H. T., "Global PNS Solutions for Transonic Strong Interaction Flows," AIAA Paper 84-0458, Jan. 1984.

[19]Barnett, M., and Davis, R. T., "Calculation of Supersonic Flows with Strong Viscous–Inviscid Interaction," *AIAA Journal*, Vol. 24, No. 12, 1986, pp. 1949–1955.

[20]Thompson, D. S., and Anderson, D. A., "A Pseudo-Unsteady Approach for Predicting Steady Supersonic Flows," AIAA Paper 87-0541, Jan. 1987.

[21]Khosla, P. K., and Rubin, S. G., "Consistent Strongly Implicit Iterative Procedures for Two-Dimensional Unsteady and Three-Dimensional Space-Marching Flow Calculations," *Computers and Fluids*, Vol. 15, No. 4, 1987, pp. 361–377.

[22]Stookesberry, D. C., and Tannehill, J. C., "Computation of Separated Flow Using the Space-Marching Conservative Supracharacteristics Method," *AIAA Journal*, Vol. 25, No. 8, 1987, pp. 1063–1070.

[23]Barnett, M., and Power, G. D., "An Efficient Algorithm for Strong Viscous/Inviscid Interaction in Hypersonic Flows," AIAA Paper 88-0712, Jan. 1988.

[24]Power, G. D., and Barber, T. J., "Analysis of Complex Hypersonic Flows with Strong Viscous/Inviscid Interaction," *AIAA Journal*, Vol. 26, No. 7, 1988, pp. 832–840.

[25]Power, G. D., "A Novel Approach for Analyzing Supersonic High Reynolds Number Flows with Separation," AIAA Paper 90-0764, Jan. 1990.

[26]Kaushik, S., and Rubin, S. G., "Primitive Variable Pressure Based Flux-Split RNS Formulations for Incompressible and Compressible Flows," AIAA Paper 95-2165, June 1995.

[27]Miller, J. H., Tannehill, J. C., and Lawrence, S. L., "Computation of Supersonic Flows with Embedded Separated Regions Using an Efficient PNS Algorithm," AIAA Paper 97-1942, June 1997.

[28]Miller, J. H., Tannehill, J. C., and Lawrence, S. L., "PNS Algorithm for Solving Supersonic Flows with Upstream Influences," AIAA Paper 98-0226, Jan. 1998.

[29]Rehyner, T. A., and Flügge-Lotz, I., "The Interaction of a Shock Wave with a Laminar Boundary Layer," *International Journal of Non-Linear Mechanics*, Vol. 3, 1968, pp. 173–199.

[30]Tannehill, J. C., Miller, J. H., and Lawrence, S. L., "Development of an Iterative PNS Code for Separated Flows," AIAA Paper 99-3361, June 1999.

[31]Tannehill, J. C., Miller, J. H., and Lawrence, S. L., "Iterative PNS Algorithms for Solving 3-D Supersonic Flows with Upstream Influences," AIAA Paper 2000-0821, Jan. 2000.

[32]Roe, P. L., "Approximate Riemann Solvers, Parameters, Vectors, and Difference Schemes," *Journal of Computational Physics*, Vol. 43, No. 2, 1983, pp. 357–372.

[33]White, F., *Viscous Fluid Flow*, McGraw–Hill, New York, 1991, pp. 514, 515.

[34]Ames Research Staff, "Equations, Tables, and Charts for Compressible Flow," NACA Rept. 1135, 1947.

[35]Chapman, D. R., Kuehn, D. M., and Larson, H. K., "Investigation of Separated Flows in Supersonic and Subsonic Streams with Emphasis on the Effect of Transition," NACA Rept. 1356, Jan. 1957.

[36]Gray, J. D., and Rhudy, R. W., "Effects of Blunting and Cooling on Separation of Laminar Supersonic Flow," *AIAA Journal*, Vol. 11, No. 9, 1973, pp. 1296–1301.

[37]Simeonides, G., Haase, W., and Manna, M., "Experimental, Analytical, and Computational Methods Applied to Hypersonic Compression Ramp Flows," *AIAA Journal*, Vol. 32, No. 2, 1994, pp. 301–310.

[38]Lewis, J. E., Kubota, T., and Lees, L., "Experimental Investigation of Supersonic Laminar, Two-Dimensional Boundary-Layer Separation in a Compression Corner with and Without Cooling," *AIAA Journal*, Vol. 6, No. 1, 1968, pp. 7–14.

[39]Hakkinen, R. J., Greber, I., Trilling, L., and Abarbanel, S. S., "The Interaction of an Oblique Shock Wave with a Laminar Boundary Layer," NASA Memo 2-18-59W, March 1959.

[40]Kaufman, L. G., II, and Johnson, C. B., "Weak Incident Shock Interactions with Mach 8 Laminar Boundary Layers," NASA TN-D-7835, Dec. 1974.

[41]Degrez, G., Boccadora, C. H., and Wendt, J. F., "The Interaction of an Oblique Shock Wave with a Laminar Boundary Layer Revisited. An Experimental and Numerical Study," *Journal of Fluid Mechanics*, Vol. 177, 1987, pp. 247–263.

[42]Carter, J. E., "Numerical Solutions of the Navier–Stokes Equations for the Supersonic Flow over a Two-Dimensional Compression Corner," NASA TR-R-385, July 1972.

[43]Hung, C. M., and MacCormack, R. W., "Numerical Solutions of Supersonic and Hypersonic Laminar Compression Corner Flows," *AIAA Journal*, Vol. 14, No. 4, 1976, pp. 475–481.

[44]Thomas, J. L., and Walters, R.W., "Upwind Relaxation Algorithms for the Navier–Stokes Equations," *AIAA Journal*, Vol. 25, No. 4, 1987, pp. 527–534.

[45]Jespersen, D. C., Pulliam, T. H., and Buning, P. G., "Recent Enhancements to OVERFLOW," AIAA Paper 97-0644, Jan. 1997.

[46]Miller, J. H., "PNS Algorithm for Solving Supersonic Flows with Upstream Influences," Ph.D. Dissertation, Dept. of Aerospace Engineering and Engineering Mechanics, Iowa State Univ., Ames, IA, Dec. 1997.

[47]Miller, J. H., Tannehill, J. C., and Lawrence, S. L., "Application of the IPNS Algorithm to Complex Two-Dimensional Body Geometries," AIAA Paper 99-0546, Jan. 1999.

D. S. McRae
Associate Editor